

Targeted Delivery of CBD-Loaded Poly(RGD) Proteinoid Nanoparticles for Antitumor Therapy

Lugasi L, Grinberg I and Margel S*

The Institute of Nanotechnology and Advanced Materials, Department of Chemistry, Bar-Ilan University, Ramat-Gan 5290002, Israel

ABSTRACT

Background: Targeted nanoparticle (NP)-based drug delivery systems enable administration of non-soluble drugs and enhance their efficacy. The arginine-glycine-aspartic acid (RGD) motif is a known recognition site of integrins, and RGD receptors are overexpressed in tumors and their neovasculature and can be used as targets for tumor treatment. Cannabidiol (CBD), the main non-psychotropic phytocannabinoid of *Cannabis sativa*, exhibits various therapeutic effects and has antitumor properties. Encapsulation of CBD within poly(RGD) (P(RGD)) proteinoid NPs can overcome the poor solubility and bioavailability of CBD and target it to tumors in vivo.

Methods: P(RGD) proteinoid polymer was synthesized from D- and L-amino acids by thermal step-growth polymerization. CBD was encapsulated within the proteinoid NPs by self-assembly process. CBD-loaded proteinoid NPs were characterized in terms of particle diameter and size distribution, drug loading, ζ -potential, cytotoxicity, drug release, and biodistribution as well as antitumor effect.

Results: P(RGD) proteinoid polymer was obtained with high molecular weight and low polydispersity. CBD was successfully encapsulated in the proteinoid NPs. The results demonstrate significant tumor growth inhibition by CBD-loaded P(RGD) proteinoid NPs compared to free CBD solution. The targeted delivery of P(RGD) NPs to tumors in a xenograft mouse model significantly increases ($p < 0.05$) the anticancer activity of CBD with respect to the free compound.

Conclusions: CBD-loaded P(RGD) NPs can potentially be used for anticancer therapy owing to their in vivo targeting ability, suggesting a good strategy for colorectal and breast cancers.

Keywords: Proteinoid nanoparticles; Self-assembly; *Cannabis sativa*; Cannabidiol; RGD motif; Drug delivery; Colorectal cancer; Breast cancer

INTRODUCTION

Cancer is one of the major diseases of the 21st century, and it is estimated that more than 24 million cases worldwide will be diagnosed until 2035 [1]. Current research shows that cancer is caused by multistep dynamic changes in the genome [2,3]. Early diagnostic technologies and the development of novel therapies considerably increased the rate of cancer survival. However, colorectal cancer (CRC) and breast cancer (BC) remain the two leading causes of cancer deaths among women worldwide [4,5]. CRC and BC are heterogeneous pathologies, divided into several subtypes according to their clinical implications, aggressiveness, presentation level, molecular characteristics, histopathology, and progressiveness of the disease [6-9]. Presently, various therapeutic approaches are used according to the cancer sub type including

surgery, hormone therapy, radiotherapy, immunotherapy and chemotherapy [10,11]. *Cannabis sativa* is known for its therapeutic and psychoactive properties for thousands of years [12]. However, only in 1960, the key ingredient Δ^9 -tetrahydrocannabinol (Δ^9 -THC) was identified and isolated by Gaoni and Mechoulam [13]. The discovery of cannabinoids, a family of active compounds with unique chemical structures in the early 1970s, was another important step in cannabis research [13]. More recently, the discovery of the endocannabinoid system and identification of its receptors CB1 and CB2 in the 1990s greatly expanded the knowledge on pharmacological effects of cannabinoids. Phytocannabinoids as well as synthetic cannabinoids were found to stimulate CB1 and CB2 and bind specific G-protein-coupled and 5-HT_{1A} serotonergic receptors of the system [14-16].

*Correspondence to: Shlomo Margel, The Institute of Nanotechnology and Advanced Materials, Department of Chemistry, Bar-Ilan University, Ramat-Gan 5290002, Israel, Tel: 97235318861; E-mail: Shlomo.margel@biu.ac.il

Received: September 01, 2020; Accepted: September 28, 2020; Published: October 01, 2020

Citation: Lugasi L, Grinberg I, Margel S (2020) Targeted Delivery of CBD-Loaded Poly (RGD) Proteinoid Nanoparticles for Antitumor Therapy. J Nanomed Nanotech. 11:552. doi: 10.35248/2157-7439.20.11.552

Copyright: ©2020 Lugasi L, et al. This is an open-access article distributed under the terms of the Creative Commons Attribution License, which permits unrestricted use, distribution, and reproduction in any medium, provided the original author and source are credited.

There is growing evidence suggesting that cannabinoids are beneficial for a wide spectrum of clinical conditions including pain [17], inflammation [18], sleep disorders [19], epilepsy [20], anorexia [21], schizophrenia [22], Parkinson's and Alzheimer's disease [23], and post-traumatic stress disorder [24].

In recent decades, an increasing number of studies on cannabidiol (CBD, Figure 1), the main nonpsychotic active compound of the cannabis plant, demonstrated that CBD and other cannabinoids have anticancer therapeutic potential, both in vitro on different cell lines and in vivo in a multitude of animal models [25]. In addition, CBD was reported to produce anti-proliferative, pro-apoptotic, cytotoxic, anti-invasive, anti-angiogenic, anti-inflammatory, and immunomodulatory effects [26,27]. Furthermore, the activation and expression of various genes, proteins, enzymes and signaling pathways by CBD at different concentrations, generates chemopreventive properties (blocking, initiation, progression and metastasizing) in different types of cancer including breast, colon, lung, prostate, skin and brain cancer, leukaemia, and cervical carcinomas [28].

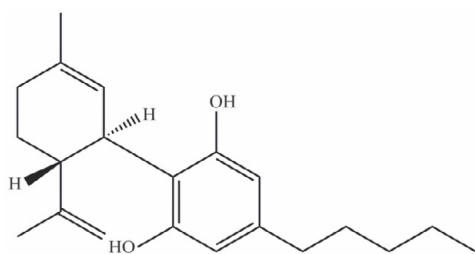


Figure 1: Chemical structure of cannabidiol (CBD).

The distribution of CBD in the body depends on age, body size, composition, and permeability of blood-tissue barriers, as it is rapidly distributed to the lungs, heart, liver and brain as well as to fatty tissues [29]. CBD is mostly metabolized by hydroxylation in the liver, and the metabolites are excreted mainly via the kidneys and urine [30]. To date, studies showed that CBD is well-tolerated and has an excellent safety profile with no reported potential hazard of physical dependence or abuse [31,32]. CBD is a solid crystalline ($M_w = 314.469 \text{ g/mol}$) with low aqueous solubility, which limits its administration [33]. It is a highly lipophilic compound with poor ($\sim 6\%$) oral bioavailability and much better bioavailability (31%) for inhalation [34]. Therefore, CBD requires alternative administration routes that increase its bioavailability and stability and improve drug efficacy.

Biodegradable nanoparticles (NPs) are known delivery systems, which increase biocompatibility, bioavailability, permeability and retention time, reduce toxicity, and pass through biological barriers [35-37]. Moreover, formulation-based biodegradable NPs are efficient drug transport systems to target sites, improve administration, and can be used to control drug targeting [35-40]. Nano-encapsulation of CBD within biodegradable polymeric NPs can improve its stability and change its biodistribution, and as a consequence, increase its availability to tumor cells.

Proteinoids are random polymers, which are synthesized by thermal step-growth polymerization [41-42]. They are biodegradable and resemble natural proteins, and thereby have non-immunogenic and non-toxic characteristics. As they are synthetic polymers, proteinoids are advantageous and can be designed according to specific properties by selecting an amino acid mixture for a particular application [43-45].

In an aqueous solution and with suitable conditions, proteinoids can self-assemble to form hollow particles [46]. The hydrophobic residues of the proteinoid form a hydrophobic core within the particle matrix to minimize their contact with the aqueous continuous phase, and the hydrophilic groups are exposed to form hydrogen bonds on the particle surface [47,48]. During the self-assembly process, the hollow interior of the particles can be exploited to encapsulate different compounds, producing proteinoid NP biocompatible drug carriers for various applications. Among these uses are anticancer drugs and near infrared (NIR) fluorescent dyes that can be potentially used for diagnosis and cancer therapy [49-51].

RGD is a cell recognition and adhesion tripeptide motif, which is exhibited in many extracellular matrix (ECM) proteins as well as in cell surface and plasma proteins [52]. RGD was first identified as a specific binding site for fibronectin and its receptors [53]. Subsequently, it attracted widespread attention and was identified with other ECM proteins [54-57]. RGD has important regulatory functions in biological pathways that involve cell attachment, cell spreading, actin skeleton formation, and focal-adhesion formation with integrins, which are important for transmitting signals related to cellular behavior and the cell cycle [58].

Integrins are transmembrane receptors that participate in cell-cell adhesion, cellular differentiation, and cell migration, facilitate cellular ECM adhesion, and are regulators of communication between cells and their microenvironment [59]. The RGD peptide increases cell adhesion and was used as an artificial ECM protein to induce specific cellular responses and promote new tissue formation [60]. In addition, it is a very well-known ligand for the extracellular domain with a high affinity to specific cancer integrin receptors in the formation of new blood vessels (angiogenesis) and is involved in processes of tumor metastasis and gene expression [61]. RGD-based targeting strategies are therefore widely used in diverse physiological and pathological processes, which mostly focus on the diagnosis and therapy of tumors (gastric, pancreatic, breast, ovarian, colon, and head and neck cancer), as well as in delivering anti-cancer drugs [62-65]. RGD functions in different strategies, which include antagonist drugs with the RGD sequence, RGD-conjugates, and grafting of RGD as a targeting ligand to the surface of nanocarriers [66].

In the present study, P(RGD) proteinoid polymer with a high molecular weight and low polydispersity were synthesized based on the assumption that step-growth polymerization will randomly form RGD sequences as part of the proteinoid backbone. Hollow and CBD-loaded P(RGD) NPs were prepared by self-assembly to overcome the stability and bioavailability challenges of CBD as well as to improve its anti-tumor therapeutic efficacy on CRC and BR cancers.

MATERIALS AND METHODS

Materials

The following analytical-grade chemicals were purchased from commercial sources and used without further purification: D-arginine (R, D-Arg), glycine (G, Gly), L-aspartic acid (D, L-Asp), sodium hydroxide (NaOH), super pure HPLC water, acetonitrile (ACN) and trifluoroacetic acid, sodium chloride (NaCl), Tween® 80, trehalose, and Cyanine7-NHS (Cy7-NHS) were all purchased in $\geq 98\%$ purity from Sigma, Israel. Cannabidiol (CBD) was kindly provided by Prof. Hinanit Kolatai (Agricultural Research

Organization, Volcani Center, Israel).

Water was purified by passing deionized water through an Elgastat Spectrum reverse osmosis system from Elga Ltd. (High Wycombe, UK). Dialysis membranes (1000 Da), Dulbecco's modified Eagle's medium, phosphate buffered saline (PBS), human serum AB (male), glutamine, penicillin/streptomycin, and cell proliferation kits (XTT based) were purchased from Biological Industries (Bet Haemek, Israel). HCT116 human colon carcinoma and MCF7 human breast adenocarcinoma cell lines were purchased from the ATCC (Manassas, VA, USA). Male BALB/C mice and athymic nude-*Foxn1*tm mice were purchased from Harlan Biotech (Rehovot, Israel).

Methods

Synthesis of P(RGD) proteinoid by thermal step-growth polymerization

The synthesis of Poly(RGD) (P(RGD)) proteinoids was carried out as previously described [67]. A mixture of 5 g of the amino acids D-Arg, Gly and L-Asp with a weight ratio of 1:1:1 was heated to 180 °C. The mixture was stirred by a mechanical stirrer at 150 rpm for 30 min and then allowed to cool to room temperature. The product was a highly viscous amber-brownish paste, which hardened upon cooling to room temperature. The residue was extracted by 30 mL of super-purified water, followed by lyophilization to yield a dried proteinoid polymer powder.

P(RGD) proteinoid characterization

The molecular weights and polydispersity indices of the dried crude proteinoids were determined at 25 °C using gel permeation chromatography (GPC) consisting of a Waters Spectra Series P100 isocratic HPLC pump with an ERMA ERC-7510 refractive index detector and a Rheodyne (Coatati, CA) injection valve with a 20 µL loop (Waters, MA). The samples were eluted with super-pure HPLC water through a linear BioSep SEC-s3000 column (Phenomenex) at a flow rate of 1 mL/min. The molecular weights of the proteinoids were determined relative to poly(ethylene glycol) standards (Polymer Standards Service-USA, Silver Spring, MD) with a molecular weight range of 100–450000 Da, human serum albumin (67 kDa) and bovine plasma fibrinogen (340 kDa), using Clarity chromatography software (DataApex, Prague, Czech Republic).

The optical activities of the proteinoids were determined using a PE 343 polarimeter (PerkinElmer). All measurements were performed in water at 589 nm and 25 °C.

Preparation of hollow and CBD-loaded P(RGD) proteinoid NPs

Proteinoid NPs were prepared via a self-assembly mechanism. Briefly, 100 mg of the dried proteinoid were added to 10 mL NaCl 10 µM aqueous solution. The mixture was then heated to 80 °C and stirred at 250 rpm for 20 min until the crude proteinoid dissolved completely. Hollow proteinoid particles were formed as the mixture was left to cool to room temperature. CBD-loaded proteinoid particles were obtained in a similar procedure by addition of CBD to the heated proteinoid solution. Due to the poor solubility of CBD in water, an appropriate concentration of CBD powder (10% w/w relative to the proteinoid) was first dissolved in ACN (0.2 mL) with 100 µL of Tween® 80 and the solution was heated. After both solutions reached 80 °C, the CBD solution was added to the proteinoid mixture prior to particle formation to achieve

CBD-loaded proteinoid NP (P(RGD)/CBD) dispersion. Following preparation, the NPs were extensively dialyzed using a cellulose dialysis membrane with a molecular weight cut-off (MWCO) of 1000 Da against distilled water to remove the ACN. The particle dispersion was filtered through a 3 µm glass microfiber membrane syringe filter (VWR EU, England) to remove excess CBD. Hollow P(RGD) NPs were prepared in the same manner without CBD.

Preparation of NIR fluorescent hollow and CBD-loaded proteinoid NPs

The NIR dye Cyanine7 NHS ester (Cy7-NHS) was conjugated to residual amine groups on the surface of the hollow and CBD-loaded proteinoid NPs. Briefly, 50 µL of the Cy7-NHS solution in DMSO (10 mg/mL) was added to the aqueously dispersed NPs and stirred at 150 rpm for 2 h at room temperature. The NIR fluorescent conjugated NP dispersion was then extensively dialyzed through a cellulose membrane (1000 Da MWCO) against distilled water to remove the DMSO and excess Cy7.

Diameter and size distribution measurements

The hydrodynamic diameter and size distribution of the aqueous NP dispersions were measured at room temperature with a particle dynamic light scattering (DLS) analyzer (Nanophox model, Sympatec GmbH, Germany). In addition, the diameter and size distribution of the NPs were measured with a cryogenic transmission electron microscope (cryo-TEM). Briefly, a small droplet of aqueous NP dispersion was placed on a perforated lacey carbon film supported on a TEM copper grid. The droplet was blotted with a piece of filter paper, resulting in the formation of thin films of 100–300 nm. The specimen was subsequently plunged into a reservoir of liquid ethane cooled by liquid nitrogen to ensure its vitrification (rapid freezing) and to prevent ice crystal formation. The vitrified specimen was transferred under liquid nitrogen and mounted on a cryogenic sample holder cooled to -170°C. All samples were observed under low-dose conditions. Vitrified samples were examined using a FEI T12 G2 Cryo-TEM operating at 120 kV and equipped with a Gatan 626 cryo-holder system. The mean diameter was determined by measuring at least 200 particles using image analysis software (AnalySIS Auto, Soft Imaging System GmbH, Germany).

ζ-Potential measurements

The surface potentials of the proteinoid NPs were measured in aqueous dispersion at a pH of 7.4 at a concentration of 10 mg/mL using a Zetasizer 3000 HSa model ζ-potential analyzer (Malvern Instruments Company, England).

High-performance liquid chromatography

High-performance liquid chromatography (HPLC) analysis of CBD drug loading (DL) was carried out using a Spectra System HPLC equipped with a UV/vis detector (Thermo Scientific, USA) and a raptor ARC-18 (150 mm × 4.6 mm, Phenomenex, USA). The mobile phase was water with 5 µM ammonium formate and acetonitrile, both containing 0.1% aqueous solution of formic acid at a flow rate of 1 mL/min at 25°C with the wavelength set at 228 nm [68]. Calibration standard solutions were prepared and used by diluting an appropriate volume of stock standard solution in ethanol, yielding concentrations of CBD in the range of 60–200 µM. CBD-loaded NPs were diluted twofold with methanol and sonicated in an ice-water bath for 20 min prior to injection to

disassemble the proteinoid NPs and elute the encapsulated CBD. The injection volume was set to 5 μ L for all standard samples in the range of 30–100 μ M CBD. The weight of drug in each sample was calculated using the calibration curve.

CBD leakage

The dialysis bag method was used to test whether there is leakage of CBD from the proteinoid particles [69]. a dialysis bag filled with 1 mL of CBD-loaded proteinoid NPs dispersion (10 mg/mL) was added into a test tube containing 50 mL of water. The test tube was placed in a refrigerator at 4°C, and the medium was tested for presence of CBD twice a week over three months by HPLC.

Long-term storage stability

Long-term storage of CBD-loaded proteinoid NPs was investigated by freeze-drying. Briefly, 10 mg of trehalose were added to 1 mL NP aqueous dispersion (10 mg/mL), followed by lyophilization to dryness and storage at 4°C. NP powder was redispersed in water to its original concentration (1 mL), and the NP diameter and size distribution were determined by DLS.

Cell viability analysis

In vitro toxicity of hollow and CBD-loaded P(RGD) NPs was tested using the XTT (2,3-bis-(2-methoxy-4-nitro-5-sulfophenyl)-2H-tetrazolium-5-carboxanilide salt) assay on two human cell lines: HCT116 colon carcinoma and MCF7 breast adenocarcinoma. Cells were seeded in a 96-well plate at a density of 1×10^4 cells/well in 100 μ L culture medium and grown in a humidified 5% CO₂ atmosphere at 37°C. Hollow and CBD-loaded P(RGD) NPs were freshly dispersed in water containing 1% ACN aqueous solution and added to a 95% confluent cell culture in culture medium. Cells were treated with proteinoid NPs at a concentration of 0.05, 0.1 and 0.5 mg/mL; free and encapsulated CBD concentration was 5, 10 or 20 μ g/mL. The cell cultures were further incubated at 37°C in a humidified 5% CO₂ incubator and examined for viability after 48 h. The percentage of cell viability was calculated as shown in the manufacturer's protocol of the XTT toxicity detection kit. Experiments were performed in triplicate, and all samples were tested in sixfold and analyzed by UV spectrophotometer at 492 nm with reference wavelength of 620 nm.

Controlled drug-release studies

In vitro drug release studies were performed by suspending nanoparticles (1 mg/mL) in human serum containing 0.5% (w/v) Tween® 80 to maintain sink conditions. Samples were incubated in a thermostatic shaking bath at $37 \pm 0.5^\circ\text{C}$ for 96 h. At predetermined time points, aliquots were removed and centrifuged through a centrifugation tube (Vivaspin 30 kDa MWCO) for 20 min, filtered using a 0.22 μ m syringe filter, and measured by HPLC as described above. Experiments were performed in triplicate.

Cell cycle studies

Cell cycle progression and apoptosis were analyzed by flow cytometry. For cell cycle analysis, 10^5 MCF7 and HCT116 cells were seeded in six-well tissue culture plates. Three days later, the cells were treated with 100 μ L of saline, P(RGD) NPs, P(RGD)/CBD NPs (containing 0.1 mg CBD), or free CBD (0.1 mg) for 24 h at 37°C. After incubation, the cells were trypsinized, counted, washed with culture medium, stained with Hoechst 33342

solution according to the manufacturer's protocol, and suspended in PBS [70]. The suspension was analyzed by flow cytometry using a BD FACSAria™ III (BD Biosciences, San Jose, CA, USA) with a 405 nm laser. A minimum of 10,000 cells were analyzed for each histogram. Gate SSC/FSC was used to exclude fragments and aggregates from the cell count. Untreated cells were used as a control. Results were analyzed using FlowJo software according to the Dean-Jett-Fox model [71].

Live cell imaging was performed on an Olympus FV-1000 confocal microscope. Briefly, 10^5 HCT116 and MCF7 cells were grown on 15 mm glass coverslips pretreated with 0.1% gelatin for 48 h. Cells were then treated with Cy7-conjugated hollow and CBD-loaded proteinoid NPs (0.1 mg/mL) for 24 h at 37°C. After incubation, the cells were washed with PBS, fixed by cold (-20°C) methanol for 20 min and stained with 4',6-diamidino-2-phenylindole (DAPI nucleus staining, Fluoroshield, Sigma).

P(RGD) NPs in vivo biodistribution studies

All animal experiments were approved by the Institutional Animal Care and Use Committee of Bar Ilan University and performed according to their guidelines and regulations (protocol reference number 15-02-2020).

Male BALB/C mice (n=36, Harlan Laboratories, Israel) were used in this study. The biodistribution of the Cy7 fluorescent RGD nanoparticles was studied in normal 8-week-old mice, weighing 20–25 g at the time of the experiment.

100 μ L of either hollow or CBD-loaded NP dispersion were administered to the mice via tail vein injection at a concentration of 1 mg/mL. Blood samples were taken immediately after NP injection and after 30, 60, 120 and 300 min. At three time points (4, 24 and 96 h post injection), mice were euthanized by CO₂, and organs were taken for imaging (brain, colon, heart, lungs, liver, spleen, kidneys, duodenum (stomach and intestine), and blood). Each group consisted of three mice.

Fluorescence images were acquired using a Maestro II in vivo fluorescence imaging system (Cambridge Research & Instrumentation, Inc., Woburn, MA) equipped with a fiber-delivered 300 W xenon excitation lamp, allowing images to be acquired from $\lambda=500$ –950 nm by a 1.3-megapixel CCD camera (Sony ICX285 CCD chip). Each pixel within the image cube has an associated fluorescence spectrum. The software for the Maestro system (Maestro 2.10.0) contains several algorithms to process the spectral data cubes to remove undesired auto-fluorescence signal and generate overlaid images for multiple fluorophores. A deep red excitation/emission filter set was used for our experiments (λ_{ex} : 700–770 nm, $\lambda_{\text{em}} > 780$ nm). The liquid crystal tunable filter was programmed to acquire image cubes from $\lambda = 780$ –840 nm with an increment of 10 nm per image. The camera was set to exposure times of 20,000 ms (brain, spleen), 5,000 ms (blood), 3,000 ms (liver, kidneys and stomach+intestine), 2,000 ms (heart), 1,000 ms (lungs), and 400 ms (colon). Fluorescence intensity measurements were performed using ImageJ NIH (National Institutes of Health) software.

In vivo therapy in athymic nude mice bearing colon and breast cancer xenografts

Six-week-old female athymic nude mice were acquired from Harlan (Israel) and allowed to acclimate one week in the animal facility before any interventions were initiated. The mice were injected

subcutaneously (SC) with HCT116 colon or MCF7 breast cancer cells (10^6 cells in 100 μL saline mixed with 100 μL Matrigel™ Basement Membrane Matrix (BD Biosciences, San Jose, CA, USA). Tumors were measured and the volume was calculated as $(\text{length} \times \text{width}^2)/2$ [72]. Treatment was initiated when tumors reached $\sim 50\text{--}100$ mm³ in volume (7–14 days after tumor cell injection), and tumor growth was monitored over time.

Twenty-four mice were randomly divided into four groups (six mice per group), and each group was treated with an injection volume of 100 μL of one of the following: PBS (normal saline), free CBD (0.1 mg CBD per injection), P(RGD) NPs (1 mg per injection), or P(RGD)/CBD NPs (0.1 mg CBD per injection). All substances were administered by IV injection via the tail vein, twice (MCF7) or three times (HCT116) per week for 7–14 days after inoculation (14–28 days after tumor cell injection). Tumor volumes and weights were monitored and compared.

All mice were observed and weighed three times a week during the study period. Four days after the last treatment, all mice were euthanized, and the tumors were carefully resected and weighed.

All data are expressed as percentage, mean with standard deviation. Statistical analysis was done using a Student's *t*-test where $p < 0.05$ was considered statistically significant.

RESULTS AND DISCUSSIONS

Cannabinoids attract great interest in cancer therapy, and several researchers developed cannabinoid-based NPs to improve their antitumor activity, including polymeric NPs [73,74]. Here we present a different system of specifically designed proteinoid NPs loaded with CBD for targeting tumor cells.

Synthesis and characterization of P(RGD) proteinoids

P(RGD) proteinoids were synthesized from the three amino acids D-Arg, Gly and L-Asp with a weight ratio of 1:1:1 by thermal step-growth polymerization process, as described in the experimental part. The concept of forming proteinoid polymers from these amino acids is based on the assumption that random polymerization will statistically yield RGD sequences as integrated parts of the proteinoid backbone. We indeed previously established the presence of RGD sequences by spectroscopic analysis [75]. Aspartic acid has to be present in the proteinoid synthesis, as at high temperatures it condenses into a succinimide, which serves as initiator and solvent for the other amino acids [76].

The P(RGD) proteinoid was characterized by its molecular weight (Mw), polydispersity index (PDI) obtained by GPC, and optical activity measured by a polarimeter, as shown in Table 1. The P(RGD) proteinoid exhibited high Mw of 186 kDa with a narrow polydispersity index (PDI) of 1.0, which is not typical for random step-growth thermal polymerization that usually attains relatively low Mw with higher PDI [50]. The high Mw indicates that during the procedure, long protein-like chains are formed, which improve the mechanical properties, resulting in multiple physical interactions between the polymer chains [77]. In addition, the chirality was not affected by the high temperatures used in the synthesis, and the proteinoids remained optically active after polymerization.

Hollow and CBD-loaded P(RGD) NP formation and characterization

As previously mentioned, proteinoids self-assemble into particles in an aqueous solution. Hollow and CBD-loaded P(RGD) particles were obtained according to the procedure in the experimental

Table 1: Composition of the P(RGD) proteinoid.

Proteinoid ^a	Amino acid ratio (w/w/w)			Proteinoid characterization				
	D-Arg	Gly	L-Asp	Mw ^b (kDa)	Mn ^b (kDa)	Mp ^b (kDa)	PDI ^c (kDa)	Optical activity [α] _D ^{25°C} (°) ^d
P(RGD)	1	1	1	186	185	187	1	-10.7

Proteinoids were prepared as described in the methods section. The total monomer weight was 5 g. ^aThe proteinoids were prepared at 180°C; ^bmolecular weights were measured by GPC, Mp is the molecular mass at the peak; ^cPDI is the polydispersity index, given by Mw/Mn; ^dspecific optical rotation ($c=1$ in H₂O at 25°C).

Table 2: Characterization of P(RGD) proteinoid NPs.

Proteinoid NPs	Diameter (nm)	ζ -potential (mV)	DL (w/w %)
P(RGD)	34 ± 3	-22.1 ± 6	-
P(RGD)/CBD	62 ± 5	-27.4 ± 5	10

Proteinoid NPs were formed by a self-assembly process in NaCl 10 μM aqueous solution containing 1% ACN. The CBD concentration was 10% w/w relative to the proteinoid. The proteinoid particle hydrodynamic diameters and SD were measured by DLS, the ζ -potential was measured at pH=7.4 by a ζ -potential analyzer, and the DL was measured by HPLC using a calibration curve of standard CBD solutions.

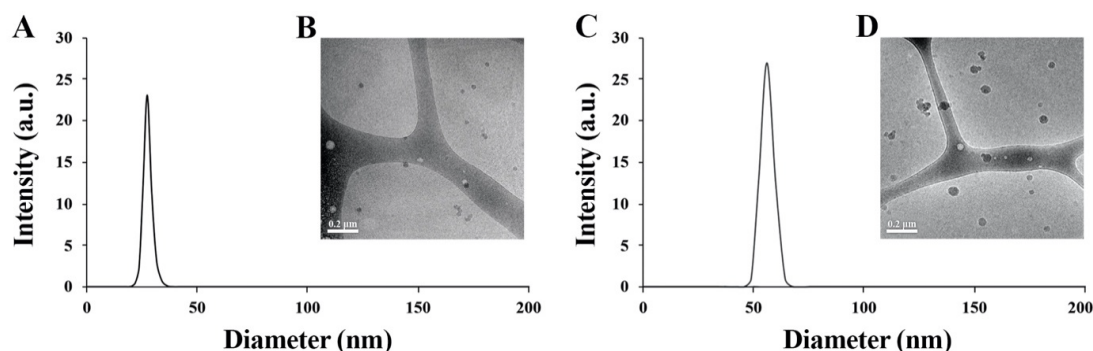


Figure 2: Hydrodynamic diameter histograms obtained by DLS and cryo-TEM images of hollow P(RGD) (A, B) and P(RGD)/CBD (C, D) nanoparticles.

part. The obtained particles were evaluated in terms of size, SD, DL and ζ -potential, see Table 2. The diameters of the hollow and CBD-loaded P(RGD) dispersed in aqueous continuous phase were analyzed by DLS and cryo-TEM, as shown in Figure 2. As expected, the diameter of the P(RGD)/CBD NPs was larger than of the hollow ones, in accord with CBD entrapment. Both P(RGD) and P(RGD)/CBD (10% w/w), exhibited populations of uniform spherical population with diameters less than 100 nm, which are typical range of NPs. Hollow P(RGD) NPs yielded hydrodynamic diameters of 34 ± 3 nm with a SD of 9%, while P(RGD)/CBD NPs had significantly larger diameters of 62 ± 5 nm with similar SD of 8%, presented by DLS histograms (Figure 2 and Table 2). Cryo-TEM microscopy demonstrated very similar particle diameters of 30 ± 2 nm with a SD of 7% and 59 ± 6 nm with a SD of 10% for hollow and CBD-loaded NPs, respectively.

ζ -Potential values predict the physical stability of NP aqueous dispersions [78]. The ζ -potential determines the degree of repulsion between close and similarly charged (either negative or positive) particles in the dispersions and indicates the probability of preventing particle aggregation. The stability of the NPs in the aqueous continuous phase at a pH of 7.4 was evaluated by ζ -potential measurements as shown in Table 2. Hollow and CBD-loaded P(RGD) NPs are acidic proteinoids and contain carboxylate groups of aspartic acid on the surface of the particles, which are exposed to the aqueous phase. Therefore, negative ζ -potential values are presented for these NPs. Very similar values of -22 ± 6 mV and -27 ± 5 mV were obtained for the P(RGD) and P(RGD)/CBD NPs, respectively, suggesting that the charge on the surface remains essentially the same after encapsulation.

The DL capacity of P(RGD) was determined by HPLC using standard calibration solutions [68]. CBD was initially dissolved in ACN (1% relative to the total aqueous dispersion volume). The result (Table 2) indicates complete encapsulation of all of the CBD (initially 10% w/w compared to the total proteinoid weight). Notably, the DL capacity remained 10% with higher initial CBD concentrations (data not shown).

CBD leakage and long-term storage stability

No leakage to the medium was detected over the course of three months, indicating that the proteinoid NPs were able to protect CBD in aqueous dispersion. However, when NPs are stored for long periods of time in aqueous media, physical instability frequently occurs, which restricts their use. To ensure long-term storage, the hollow and CBD-loaded proteinoid dispersions were freeze-dried in the presence of 1% (w/v) trehalose, a natural

alpha-linked disaccharide known to prevent denaturation and aggregation of proteins while preserving their natural form [79]. In the absence of trehalose, proteinoid NPs could not be freeze-dried and then redispersed [80]. After the NPs were lyophilized and redispersed in an aqueous phase, the particle size and DL capacity were maintained. Moreover, this was also the case when the NPs were redispersed at higher concentrations, above the initial concentration of 10 mg/mL.

In vitro cell viability assay

XTT-based cell viability assays are used in cell culture to study changes in the number of cells and their metabolic activity. This provides insights into cell viability, cell proliferation, and cytotoxicity. The XTT assay is based on the extracellular reduction of XTT by NADH produced in the mitochondria via trans-plasma membrane electron transport and an electron mediator. The effects of P(RGD) and P(RGD)/CBD proteinoid NPs on HCT116 human colon carcinoma and MCF7 human breast adenocarcinoma cell lines were tested with different NP concentrations (0.05, 0.1 and 0.5 mg/mL) using XTT, as described in the methods section (Figure 3A). A positive control (cells and medium only) exhibited cell viability of $102 \pm 6\%$ (HCT116) and $100 \pm 4\%$ (MCF7), and a negative control (medium only) showed 0% viability.

Free CBD and hollow P(RGD) NPs did not exert any cytotoxic effect on HCT116, showing a similar cell viability of $102 \pm 3\%$ and $101 \pm 2\%$, respectively, even after treating the cells with a high dose of 20 $\mu\text{g/mL}$. However, P(RGD)/CBD NPs exhibited cytotoxic effects on these cells with low cell viability levels of $6 \pm 2\%$, $4 \pm 1\%$ and $7 \pm 3\%$ at concentrations of 5, 10 and 20 $\mu\text{g/mL}$, respectively.

Similar effects were shown for MCF7 cells. Free CBD and hollow P(RGD) NPs displayed cell viabilities of $98 \pm 1\%$ and $101 \pm 2\%$, respectively, while P(RGD)/CBD NPs showed a cell viability of $2 \pm 0.3\%$ at a low concentration of 5 $\mu\text{g/mL}$, and similar cytotoxicity of $2 \pm 1\%$ and $3 \pm 1\%$ at concentrations of 10 $\mu\text{g/mL}$ and 20 $\mu\text{g/mL}$, respectively.

This cytotoxic effect in both HCT116 and MCF7 cells demonstrates that CBD loaded within P(RGD) NPs presents significantly high cytotoxicity compared with essentially no cytotoxicity for similar concentration of free CBD. This is probably due to the ability of CBD to penetrate and destroy tumor cells efficiently when encapsulated in P(RGD) nanoparticles.

Controlled drug-release study

An in vitro drug release study was performed in human serum at

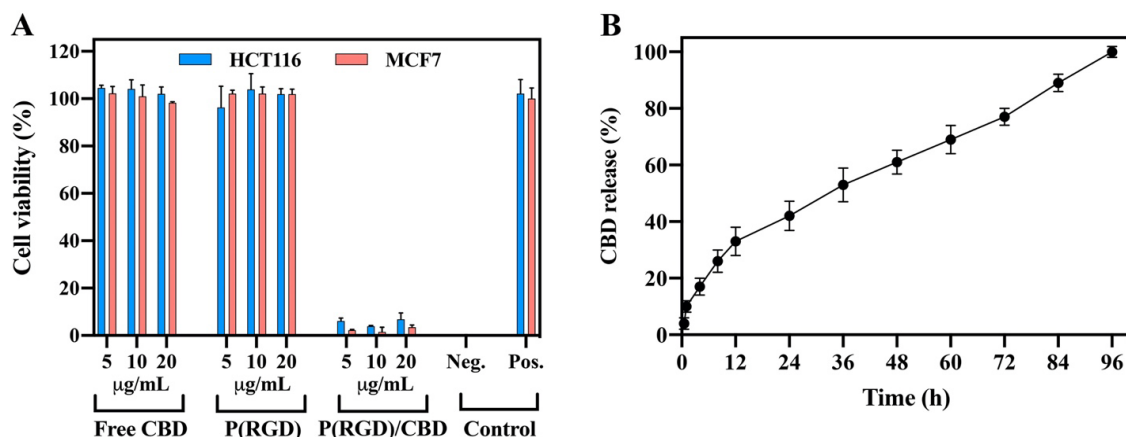


Figure 3: In vitro studies of CBD loaded P(RGD) NPs. (A) XTT cell viability assay in human HCT116 colon carcinoma and MCF7 breast adenocarcinoma cells following a 48 h exposure to hollow and CBD-loaded P(RGD) NPs. (B) Controlled-release study of CBD-loaded P(RGD) NPs in human serum.

37°C for 96 h, as described in Figure 3B. Human serum contains a high concentration of active enzymes (proteolytic enzymes and esterases), which break the peptide and ester bonds of the proteinoid polymer. We detected a controlled-release of CBD over a period of 96 h, with 100% CBD released by this time. A high burst effect was observed during the first 12 h in which 33% of the CBD was released, with a gradual release during the remainder of the experiment. Therefore, it is likely that a single administration of this nano-formulation would provide a constant CBD release for 96 h. However, faster release is expected due to the acidic ECM pH value (~5.5–6.8) in tumor cells.

In vitro cell cycle and uptake studies of hollow and CBD-loaded P(RGD) NPs

Cell permeability of Cy7-conjugated hollow and CBD-loaded P(RGD) NPs was evaluated in HCT116 and MCF7 cells using fluorescence-activated cell sorting (FACS) analysis. The NIR dye Cy7 was conjugated to the surface of the NPs to assess cellular uptake. Figure 4A and C presents the intracellular fluorescence 4 h post-uptake, showing slightly higher signals for CBD-loaded vs. hollow NPs.

Fluorescence microscopy images of the Cy7-conjugated hollow P(RGD) NPs were visualized by confocal microscope. Cell nuclei were stained with Hoechst 33342 [81]. Figure 4B and D present the intracellular fluorescence in HCT116 and MCF7, respectively, demonstrating that following 24 h of incubation, the NPs penetrate the cells and reach the cytoplasm. These results support

the hypothesis that proteinoid NPs resemble proteins and can therefore be transported across the cell membrane in a similar manner.

The effect of CBD-loaded P(RGD) NPs on the cell cycle was compared to free CBD and studied using flow cytometry, as shown in Figure 5. Human HCT116 and MCF7 cells were incubated with free and encapsulated CBD at 10 µg/ml for 24 h. Free CBD demonstrated no effect on cell cycle, with 35/51% of the cells in G1 phase in treated HCT116/MCF7 cells vs. 33/48% in untreated cells. However, treatment with CBD-loaded P(RGD) NPs exhibited an increase in G1 phase to 48/59% in HCT116/MCF7 cells, in accord with the expected increase in intracellular CBD concentration in samples treated with P(RGD)/CBD NPs compared to free CBD, suggesting a more efficient cellular uptake.

In addition, the number of MCF7 cells in the S phase increased significantly (41%) after uptake of P(RGD)/CBD NPs. The percentage of cells in G2 phase in this group was only 3%. These results also demonstrate that the CBD-loaded NPs influence the cell cycle.

In vivo biodistribution study of P(RGD) NPs

To determine the in vivo body distribution and blood half-life ($t_{1/2}$) of Cy7-conjugated P(RGD) NPs, 100 µL of NPs at a concentration of 1 mg/mL were IV injected into the tail vein of male BALB/C mice. Blood was drawn at 0, 30 min, 1 h and 2 h post injection. The results (Figure 6A) clearly show that by 30 min most of the injected quantity of the fluorescent NPs is cleared from

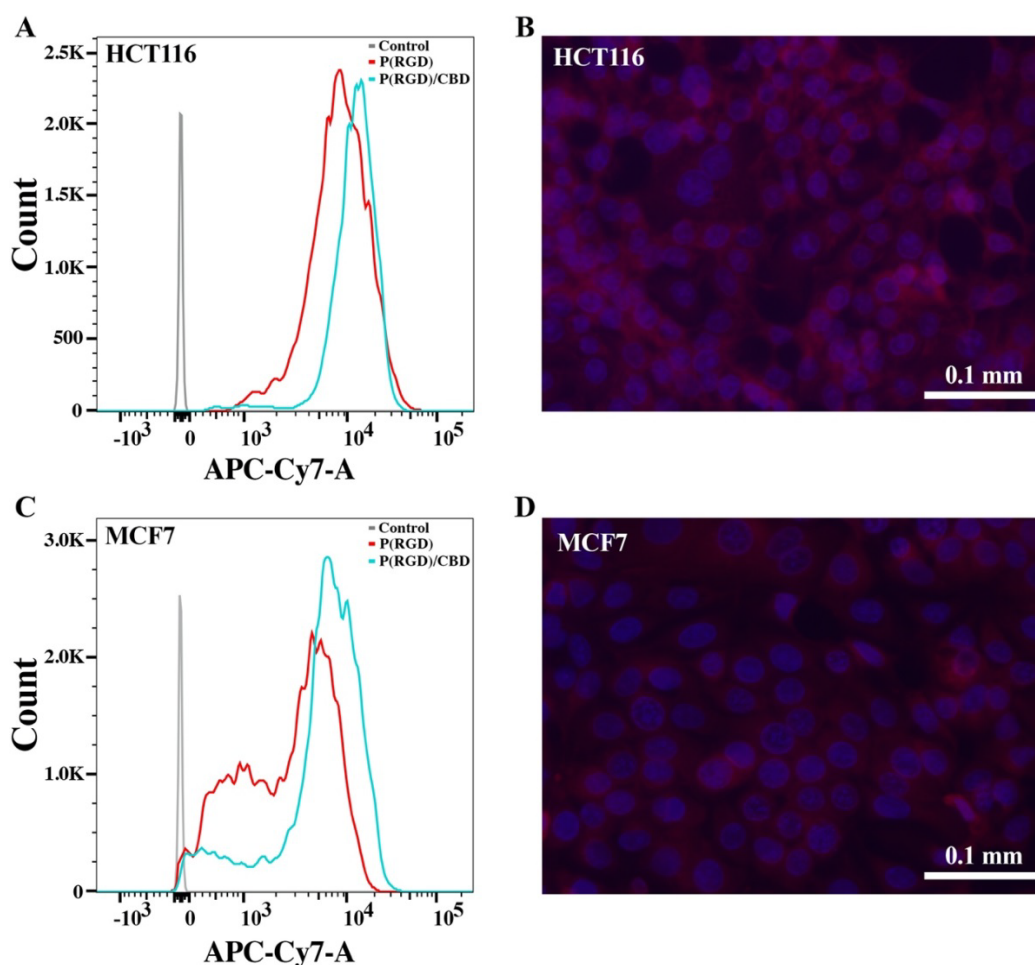


Figure 4: Cell permeability of Cy7-conjugated P(RGD) NPs. Slightly lower intracellular fluorescence is seen in cells treated with hollow vs. CBD-loaded NPs for 24 h in both HCT116 (A) and MCF7 cells (C). Fluorescence microscopy images of cell membrane (red) and nucleus (Hoechst dye, blue) show P(RGD) cellular uptake in HCT116 (B) and MCF7 (D) cells following 24 h exposure.

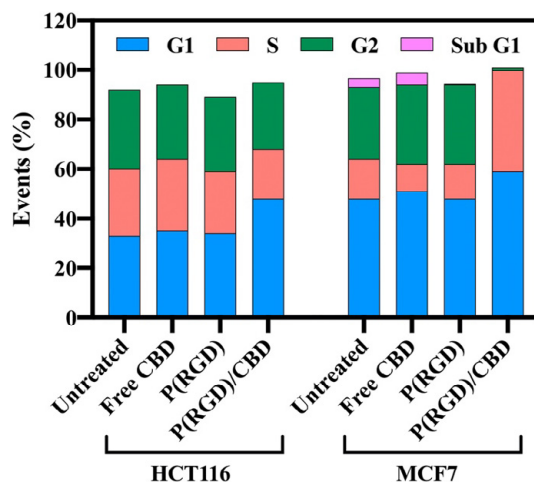


Figure 5: Cell cycle phase of HCT116 and MCF7 cells treated with free CBD, P(RGD) and P(RGD)/CBD nanoparticles for 24 h.

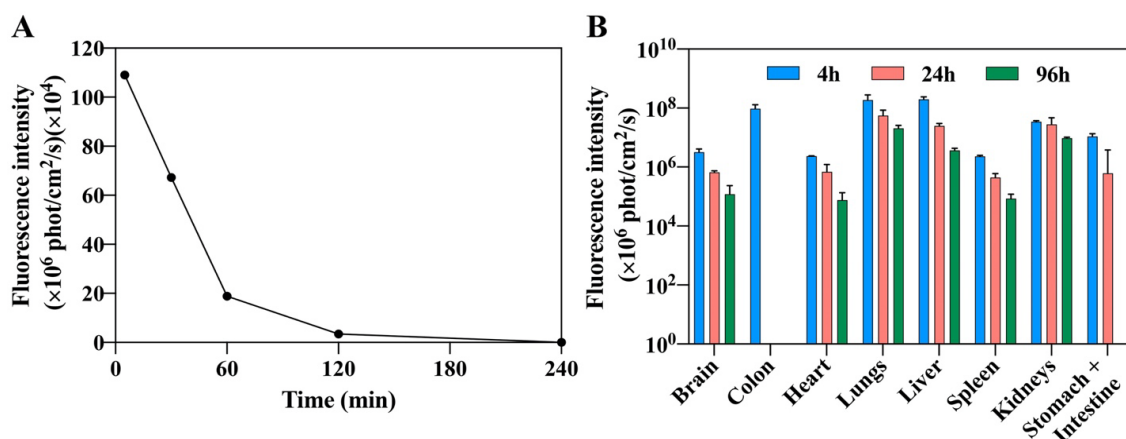


Figure 6: Biodistribution studies of P(RGD) proteinoid NPs. Blood clearance was determined after IV injection of Cy7-conjugated NPs into the tail vein (100 μ L at 1 mg/mL) by drawing blood at different time intervals and measuring the fluorescence (A). Organs were harvested at 4, 24 and 96 h post injection, and the fluorescence was measured (B).

the blood. $T_{1/2}$ is approximately 12 min. Mice were sacrificed, and several organs were harvested at 4, 24 and 96 h post injection, and their fluorescence intensity was measured using the Maestro II in vivo imaging system. Figure 6B shows that P(RGD) NPs penetrated and were found in all harvested organs. P(RGD) NPs were mostly concentrated in the liver and lungs and were probably evacuated from the body through the liver-intestine-colon and kidneys-urine routes. Interestingly, it is also apparent that some NPs pass the blood-brain barrier (BBB), as they were found in the brain at all time points post injection ($\approx 0.6\%$ of total tested organ fluorescence after 4 h). Therefore, P(RGD) NPs can potentially be used as a drug delivery system to the brain, allowing drug targeting to the brain of therapeutic molecules that usually do not pass the BBB. Overall, it was demonstrated that following a single IV injection of P(RGD) NPs, fluorescence intensity in all organs decreased over time.

In vivo therapeutic activity of CBD-loaded P(RGD) NPs on human HCT116 and MCF7 tumors in a nude mouse model

The anti-cancer effect of CBD-loaded P(RGD) NPs in human HCT116 and MCF7 cell xenograft tumors was studied in a nude mouse model. The mice were treated with 100 μ L injection volume of either PBS, hollow P(RGD) NPs, P(RGD)/CBD NPs, or free CBD via an IV injection into the tail vein, as described in the methods section. When the tumor volumes of the control mice reached 50–100 mm³, the effect of the NPs on tumor growth (volume and weight) was compared. It should be noted that the weight of the mice during the experiment was normal.

The tumor volumes of HCT116 and MCF7 during the experiment are shown in Figure 7A and C, respectively. The results demonstrate that in the last two measurement, the treatment with P(RGD)/CBD NPs significantly suppressed HCT116 tumor growth (770 \pm 141 mm³/P(RGD)/CBD vs. 980 \pm 128 mm³/PBS, $p < 0.03$ and 1000 \pm 342 mm³/P(RGD)/CBD vs. 1590 \pm 257 mm³/PBS, $p < 0.01$). Similar results are presented for MCF7 (79 \pm 15 mm³/P(RGD)/CBD vs. 101 \pm 17 mm³/PBS, $p < 0.04$ and 92 \pm 19 mm³/P(RGD)/CBD vs. 139 \pm 28 mm³/PBS for MCF7, $p < 0.01$). In addition, the tumor volume did not exhibit significant changes when treated with free CBD.

The obtained tumor weights demonstrate no change following treatment with free CBD (0.1 mg per injection), indicating no cytotoxic effect on HCT116 and MCF7 subcutaneous tumor growth (Figure 7B and C, respectively).

Figure 7B and C exhibit the mean tumor weights for P(RGD)/CBD NPs injected into mice with HCT116 and MCF7 cells, respectively; the weights were significantly lower (0.6 \pm 0.13 g for HCT116, $p < 0.04$ and 0.18 \pm 0.05 g for MCF7, $p < 0.04$) than those of tumors treated with hollow P(RGD) NPs, free CBD, or saline (1 \pm 0.4 g for HCT116 and 0.28 \pm 0.08 g for MCF7). The observed results support the importance of encapsulating CBD within P(RGD) proteinoid NPs. The reduction in tumor weight is most probably due to the RGD sequence, which binds to the tumor cells, thereby targeting CBD directly to these cells.

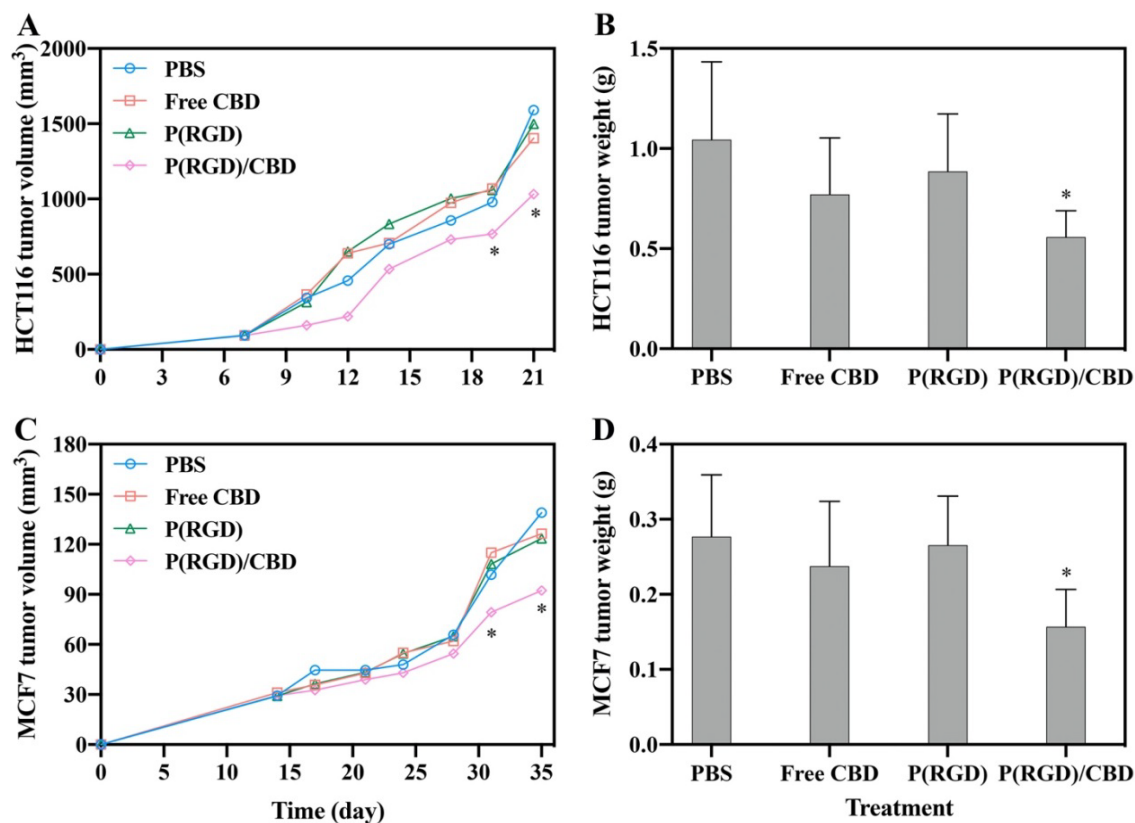


Figure 7: Effect on tumor volume and weight in subcutaneous xenograft tumors in nude mouse model in HCT116 (A,B) and MCF7 (C,D) cells following 100 μ L bi/tri-weekly IV injection for 14 days of PBS, free CBD (0.1 mg CBD per injection), P(RGD) NPs (1 mg per injection), and P(RGD)/CBD NPs (0.1 mg CBD per injection). *T-test $p < 0.05$ and error bars represent standard deviations.

CONCLUSIONS

In this study, we investigated a new drug delivery system for CBD as an anti-cancer agent for colorectal and breast cancers. For this purpose, acidic proteinoids were synthesized from D-Arg, Gly and L-Asp via thermal step-growth polymerization. The main concept for choosing these amino-acids is to form RGD motifs within the polymer backbone in order to increase the binding affinity of the NPs to the tumor cells as recently demonstrated by our group [75]. The obtained proteinoid polymer was uniform in size and with a relatively high molecular weight. Empty and CBD (10% w/w)-loaded proteinoid NPs were prepared by a self-assembly process and characterized in terms of diameter, ζ -potential, and DL. Nanosized particles measuring 97 ± 4 nm and 86 ± 3 nm, were obtained for empty and CBD-loaded NPs, respectively. HPLC measurements confirmed that CBD was successfully loaded within the proteinoid NPs, and DL analysis exhibited 100% encapsulation. Furthermore, long-term storage showed that particles after undergoing a freeze-drying process in the presence of 1% w/v trehalose, redispersed successfully to their original size.

In vitro studies of cytotoxicity and NP cell uptake were examined by XTT, FACS, cell cycle analysis, and fluorescence microscopy. It was demonstrated that hollow NPs are nontoxic, penetrate the cell membrane and reach the cytoplasm. While free CBD was also nontoxic, similar concentrations of encapsulated CBD showed high toxicity, in accord with its expected ability to efficiently penetrate and destroy tumor cells due to the encapsulating RGD motif.

A drug release study of CBD was also performed, showing a high burst effect during the first 12 h in which about a third of the CBD was released, with a gradual release over 84 h. Faster release is expected due to the acidic ECM in tumor cells. An in vivo bio

distribution study demonstrated that P(RGD) NPs were distributed in all examined organs, including the brain.

We have shown the potential use of CBD-loaded P(RGD) NPs for targeting and treating CRC and BR cancer. The RGD motif, which has a high affinity to tumor receptors and blood vessels possibly enables the delivery of CBD directly to the tumor. The intention of this study was to assess two aspects – the short-term targeting of P(RGD) NPs, and the potential therapeutic encapsulation of CBD using these novel NPs. The results reveal that the targeted delivery of CBD significantly increases its anticancer efficacy, allowing lower concentrations. While further studies are necessary, this work supports the notion that P(RGD) proteinoid NPs offer a viable and potentially good strategy for administration of CBD for colorectal and breast cancer treatment. Furthermore, these NPs may be applied for other cancer models as well.

ACKNOWLEDGEMENTS

The authors thank Dr. Alexander Varvak for his assistance with the HPLC analysis. The authors would like to thank Dr. Yuval Elias and Dr. Mechael Kanovsky for scientific editing of the manuscript.

AUTHORS' CONTRIBUTIONS

LL designed research, prepared, characterized and investigated the NPs, performed and analyzed the in vitro and in vivo experiments, and drafted and edited the manuscript. IG planned, performed and analyzed the in vitro and in vivo experiments. SM, principal investigator.

All authors read and approved the final manuscript.

SOURCES OF FUNDING

This research received no external funding.

CONFLICT OF INTERESTS

The authors declare that they have no competing interests.

REFERENCES

- Pilleron S, Sarfati D, Janssen-Heijnen M, Vignat J, Ferlay J, Bray F, et al. Global cancer incidence in older adults, 2012 and 2035: a population-based study. *Int J Cancer* 2019; 144: 49–58.
- Ponder BA. Cancer genetics. *Nature* 2001; 411: 336–341.
- Futreal PA, Coin L, Marshall M, Down T, Hubbard T, Wooster R, et al. A census of human cancer genes. *Nat Rev Cancer* 2004; 4: 177–183.
- Siegel RL, Miller KD, Fedewa SA, Ahnen DJ, Meester RGS, Barzi A, et al. Colorectal cancer statistics, 2017. *CA Cancer J Clin* 2017; 6: 177–193.
- Ng ZX, Ong MS, Jegadeesan T, Deng S, Yap CT. Breast cancer: exploring the facts and holistic needs during and beyond treatment. *Healthcare* 2017; 5: 26.
- Fedele M, Cerchia L, Chiappetta G. The epithelial-to-mesenchymal transition in breast cancer: focus on basal-like carcinomas. *Cancers* 2017; 9: 134.
- Dai X, Li T, Bai Z, Yang Y, Liu X, Zhan J, et al. Breast cancer intrinsic subtype classification, clinical use and future trends. *Am J Cancer Res* 2015; 5: 2929–2943.
- Linnekamp JF, Wang X, Medema JP, Vermeulen L. Colorectal cancer heterogeneity and targeted therapy: a case for molecular disease subtypes. *Cancer Res* 2015; 75: 245–249.
- Markowitz SD, Bertagnolli MM. Molecular origins of cancer: molecular basis of colorectal cancer. *N Engl J Med* 2009; 361: 2449–2460.
- Waks AG, Winer EP. Breast cancer treatment: a review. *JAMA* 2019; 321: 288–300.
- Haraldsdottir S, Einarsdottir HM, Smaradottir A, Gunnlaugsson A, Halfdanarson TR. Colorectal cancer - review. *Laeknabladid* 2014; 100: 75–82.
- Pertwee RG. *Handbook of cannabis*. Oxford: Oxford University Press; 2014.
- Gaoni Y, Mechoulam R. Isolation, structure, and partial synthesis of an active constituent of hashish. *J Am Chem Soc* 1964; 86: 1646–1647.
- ElSohly MA, Radwan MM, Gul W, Chandra S, Galal A. Phytochemistry of *Cannabis sativa* L. *Prog Chem Org Nat Prod* 2017; 103: 1–36.
- Kumar A, Premoli M, Aria F, Bonini SA, Maccarinelli G, Gianoncelli A, et al. Cannabimimetic plants: are they new cannabinoidergic modulators? *Planta* 2019; 249: 1681–1694.
- Pisanti S, Bifulco M. Modern history of medical cannabis: from widespread use to prohibitionism and back. *Trends Pharmacol Sci* 2017; 38: 195–198.
- Mallick-Searle T, St. Marie B. Cannabinoids in pain treatment: an overview. *Pain Manag Nurs* 2019; 20: 107–112.
- Perisetti A, Rimu AH, Khan SA, Bansal P, Goyal H. Role of cannabis in inflammatory bowel diseases. *Ann Gastroenterol* 2020; 33: 134–144.
- Suraev AS, Marshall NS, Vandrey R, McCartney D, Benson MJ, McGregor IS, et al. Cannabinoid therapies in the management of sleep disorders: a systematic review of preclinical and clinical studies. *Sleep Med Rev* 2020; 53: 101339.
- Morano A, Fanella M, Albin M, Cifelli P, Palma E, Giallonardo AT, et al. Cannabinoids in the treatment of epilepsy: current status and future prospects. *Neuropsychiatr Dis Treat* 2020; 16: 381–396.
- Rosager EV, Møller C, Sjögren M. Treatment studies with cannabinoids in anorexia nervosa: a systematic review. *Eat Weight Disord - Stud Anorexia, Bulim Obes* 2020.
- Khan R, Naveed S, Mian N, Fida A, Raafey MA, Aedma KK. The therapeutic role of Cannabidiol in mental health: a systematic review. *J Cannabis Res* 2020; 2: 2.
- Mannucci C, Navarra M, Calapai F, Spagnolo E V, Busardò FP, Cas RD, et al. Neurological aspects of medical use of cannabidiol. *CNS Neurol. Disord. - Drug Targets* 2017; 16: 541–553.
- Hindocha C, Cousijn J, Rall M, Bloomfield MAP. The effectiveness of cannabinoids in the treatment of posttraumatic stress disorder (PTSD): a systematic review. *J Dual Diagn.* 2020; 16: 120–139.
- Ramer R, Hinz B. Cannabinoids as anticancer drugs. *Adv Pharmacol.* 2017; 80: 397–436.
- Fraguas-Sánchez AI, Martín-Sabroso C, Torres-Suárez AI. Insights into the effects of the endocannabinoid system in cancer: a review. *Br J Pharmacol.* 2018 1; 175:2566–2580.
- Elanne C, Adriana I, Juliana F, Raphael S. Biological properties and therapeutic applications of cannabidiol. *J Med Plants Res.* 2020; 14: 283–291.
- Kis B, Ifrim FC, Buda V, Avram S, Pavel IZ, Antal D, et al. Cannabidiol-from plant to human body: a promising bioactive molecule with multi-target effects in cancer. *Int J Mol Sci* 2019; 20: 5905.
- Martin JH, Schneider J, Lucas CJ, Galettis P. Exogenous cannabinoid efficacy: merely a pharmacokinetic interaction? *Clin Pharmacokinet.* 2018; 57: 539–545.
- Huestis MA. Human Cannabinoid pharmacokinetics. *Chem Biodivers* 2007; 4: 1770–804.
- Bergamaschi MM, Queiroz RHC, Zuardi AW, Crippa JAS. Safety and side effects of cannabidiol, a *Cannabis sativa* constituent. *Curr Drug Saf* 2011; 6: 237–249.
- Iffland K, Grotenhermen F. An update on safety and side effects of cannabidiol: a review of clinical data and relevant animal studies. *Cannabis Cannabinoid Res* 2017 1; 2: 139–154.
- Lucas CJ, Galettis P, Schneider J. The pharmacokinetics and the pharmacodynamics of cannabinoids. *Br J Clin Pharmacol* 2018; 84: 2477–2482.
- Ohlsson A, Lindgren J-E, Andersson S, Agurell S, Gillespie H, Hollister LE. Single-dose kinetics of deuterium-labelled cannabidiol in man after smoking and intravenous administration. *Biomed Environ Mass Spectrom* 1986; 13: 77–83.
- Lu Y, Chen SC. Micro and nano-fabrication of biodegradable polymers for drug delivery. *Adv Drug Deliv Rev* 2004; 56: 1621–33.
- Karlsson J, Vaughan HJ, Green JJ. Biodegradable polymeric nanoparticles for therapeutic cancer treatments. *Annu Rev Chem Biomol Eng* 2018; 9: 105–27.
- George A, Shah PA, Shrivastav PS. Natural biodegradable polymers based nano-formulations for drug delivery: a review. *Int J Pharm* 2019; 561: 244–64.
- Leone-Bay A, McInnes C, Wang NF, DeMorin F, Achan D, et al. Microsphere formation in a series of derivatized α -amino acids: properties, molecular modeling, and oral delivery of salmon calcitonin. *J Med Chem* 1995; 38: 4257–4262.
- Leone-bay, A., Santiago N. N-Acylated alpha-amino acids as novel oral delivery agents for proteins. *J Med Chem* 1995; 38: 4263–9.
- Hans ML, Lowman AM. Biodegradable nanoparticles for drug delivery

- and targeting. *Curr Opin Solid State Mater Sci.* 2002; 6: 319–27.
41. Fox SW, Harada K. The thermal copolymerization of amino acids common to protein. *J Am Chem Soc* 1960; 82: 3745–3751.
 42. Fox SW, Nakashima T, Przybylski A, Syren RM. The updated experimental proteinoid model. *Int J Quantum Chem* 1982; 22: 195–204.
 43. Kumar AA, Karthick K, Arumugam KP. Properties of biodegradable polymers and degradation for sustainable development. *Int J Chem Eng Appl.* 2011; 2: 164–7.
 44. Kile S, Koltitz-Domb M, Corem-Salkmon E, Margel S. Engineered doxorubicin delivery system using proteinoid-poly (L-lactic acid) polymeric nanoparticles of narrow size distribution and high molecular weight for cancer treatment. *Int J Nanotechnol Nanomedicine* 2017; 2: 1–11.
 45. Koltitz-Domb M, Margel S. Recent advances of novel proteinoids and proteinoid nanoparticles and their applications in biomedicine and industrial uses. *Isr J Chem* 2018; 58: 1277–85.
 46. Syren RM, Sanjur A, Fox SW. Proteinoid microspheres more stable in hot than in cold water. *BioSystems* 1985; 17: 275–80.
 47. Madhan Kumar AB, Panduranga Rao K. Preparation and characterization of pH-sensitive proteinoid microspheres for the oral delivery of methotrexate. *Biomaterials* 1998; 19: 725–32.
 48. Urry DW, Channe Gowda D, Peng SQ, Parker TM. Non-linear hydrophobic-induced pKa shifts: implications for efficiency of conversion to chemical energy. *Chem Phys Lett* 1995; 239: 67–74.
 49. Koltitz-Domb M, Corem-Salkmon E, Grinberg I, Margel S. Synthesis and characterization of bioactive conjugated near-infrared fluorescent proteinoid-poly (L-lactic acid) hollow nanoparticles for optical detection of colon cancer. *Int J Nanomedicine* 2014; 9: 5041–53.
 50. Koltitz-Domb M, Grinberg I, Corem-Salkmon E, Margel S. Engineering of near infrared fluorescent proteinoid-poly (L-lactic acid) particles for in vivo colon cancer detection. *J Nanobiotechnology* 2014; 12: 30–43.
 51. Quirk S. Enhanced catalytic activity from proteinoid microspheres. *J Biomed Mater Res Part A* 2013; 101A: 1133–43.
 52. Colombo M, Bianchi A. Click chemistry for the synthesis of RGD-containing integrin ligands. *Molecules* 2010; 15: 178–97.
 53. Pierschbacher MD, Ruoslahti E. Cell attachment activity of fibronectin can be duplicated by small synthetic fragments of the molecule. *Nature* 1984; 309: 30–3.
 54. Suzuki S, Oldberg A, Hayman EG, Pierschbacher MD, Ruoslahti E. Complete amino acid sequence of human vitronectin deduced from cDNA. Similarity of cell attachment sites in vitronectin and fibronectin. *EMBO J* 1985; 4: 2519–24.
 55. Plow EF, Pierschbacher MD, Ruoslahti E, Marguerie GA, Ginsberg MH. The effect of Arg-Gly-Asp-containing peptides on fibrinogen and von Willebrand factor binding to platelets. *Proc Natl Acad Sci USA* 1985; 82: 8057–61.
 56. Oldberg A, Franzén A, Heinegård D. Cloning and sequence analysis of rat bone sialoprotein (osteopontin) cDNA reveals an Arg-Gly-Asp cell-binding sequence. *Proc Natl Acad Sci USA* 1986; 83: 8819–23.
 57. Grant DS, Tashiro K, Segui-Real B, Yamada Y, Martin GR, Kleinman HK. Two different laminin domains mediate the differentiation of human endothelial cells into capillary-like structures in vitro. *Cell* 1989; 58: 933–43.
 58. Hwang DS, Sim SB, Cha HJ. Cell adhesion biomaterial based on mussel adhesive protein fused with RGD peptide. *Biomaterials.* 2007; 28: 4039–46.
 59. Yamada KM, Geiger B. Molecular interactions in cell adhesion complexes. *Curr Opin Cell Biol* 1997; 9: 76–85.
 60. Bellis SL. Advantages of RGD peptides for directing cell association with biomaterials. *Biomaterials* 2011; 32: 4205–10.
 61. Humphries JD, Byron A, Humphries MJ. Integrin ligands at a glance. *J Cell Sci* 2006; 119: 3901–3.
 62. Ju JA, Godet I, Ye IC, Byun J, Jayatilaka H, Lee SJ, et al. Hypoxia selectively enhances integrin $\alpha(5)\beta(1)$ receptor expression in breast cancer to promote metastasis. *Mol Cancer Res* 2017; 15: 723–34.
 63. Mitjans F, Meyer T, Fittschen C, Goodman S, Jonczyk A, Marshall JF, et al. In vivo therapy of malignant melanoma by means of antagonists of alphav integrins. *Int J cancer* 2000; 87: 716–23.
 64. Bates RC, Bellovin DI, Brown C, Maynard E, Wu B, Kawakatsu H, et al. Transcriptional activation of integrin beta6 during the epithelial-mesenchymal transition defines a novel prognostic indicator of aggressive colon carcinoma. *J Clin Invest* 2005; 115: 339–47.
 65. Böger C, Warneke VS, Behrens H-M, Kalthoff H, Goodman SL, Becker T, et al. Integrins $\alpha v \beta 3$ and $\alpha v \beta 5$ as prognostic, diagnostic, and therapeutic targets in gastric cancer. *Gastric cancer* 2015; 18: 784–95.
 66. Jin H, Varner J. Integrins: roles in cancer development and as treatment targets. *Br J Cancer* 2004; 90: 561–5.
 67. Koltitz-Domb M, Margel S. Engineering of novel proteinoids and PLLA-proteinoid polymers of narrow size distribution and uniform nano/micro-hollow particles for biomedical applications. in: P Sera, Andrea (Ed.), *Adv Bioeng* 2015; 51–77.
 68. Restek Corporation. The LC-UV analysis of 16 cannabinoids of interest in commercially available CBD oils. 2017.
 69. Das S, Ng WK, Kanaujia P, Kim S, Tan RBH. Formulation design, preparation and physicochemical characterizations of solid lipid nanoparticles containing a hydrophobic drug: effects of process variables. *Colloids Surfaces B Biointerfaces* 2011; 88: 483–9.
 70. Chazotte B. Labeling nuclear DNA with hoechst 33342. *Cold Spring Harb Protoc* 2011.
 71. Fox MH. A model for the computer analysis of synchronous DNA distributions obtained by flow cytometry. *Cytometry* 1980; 1: 71–7.
 72. Jensen MM, Jørgensen JT, Binderup T, Kjaer A. Tumor volume in subcutaneous mouse xenografts measured by microCT is more accurate and reproducible than determined by 18F-FDG-microPET or external caliper. *BMC Med Imaging* 2008; 8: 16.
 73. Martín-Banderas L, Muñoz-Rubio I, Álvarez-Fuentes J, Durán-Lobato M, Arias JL, Holgado MÁ, et al. Engineering of $\Delta 9$ -tetrahydrocannabinol delivery systems based on surface modified-PLGA nanoplatforms. *Colloids Surfaces B Biointerfaces* 2014; 123: 114–22.
 74. Martín-Banderas L, Muñoz-Rubio I, Prados J, Álvarez-Fuentes J, Calderón-Montañó JM, López-Lázaro M, et al. In vitro and in vivo evaluation of $\Delta 9$ -tetrahydrocannabinol/PLGA nanoparticles for cancer chemotherapy. *Int J Pharm* 2015; 487: 205–12.
 75. Hadad E, Rudnick-Glick S, Grinberg I, Koltitz-Domb M, Chill JH, Margel S. Synthesis and characterization of poly(RGD) proteinoid polymers and NIR fluorescent nanoparticles of optimal D,L-configuration for drug delivery applications—in vitro study. *ACS Omega* 2020; 5: 23568–23577.
 76. Harada K, Fox SW. The Thermal condensation of glutamic acid and glycine to linear peptides. *J Am Chem Soc* 1958; 80: 2694–7.
 77. Shikanov A, Kumar N, Domb AJ. Biodegradable polymers: an update. *Isr J Chem* 2005; 45: 393–9.
 78. Shah R, Eldridge D, Palombo E, Harding I. Optimisation and stability assessment of solid lipid nanoparticles using particle size and zeta potential. *J Phys Sci* 2014; 25: 59–75.
 79. Jain NK, Roy I. Effect of trehalose on protein structure. *Protein Sci* 2009; 18: 24–36.

80. Ma X, Santiago N, Chen YS, Chaudhary K, Milstein SJ, Baughman RA. Stability study of drug-loaded proteinoid microsphere formulations during freeze-drying. *J Drug Target* 1994; 2: 9-21.
81. Latt SA, Stetten G, Juergens LA, Willard HF, Scher CD. Recent developments in the detection of deoxyribonucleic acid synthesis by 33258 Hoechst fluorescence. *J Histochem Cytochem* 1975; 23: 493-505.